JOURNAL OF ROCK MECHANICS

VOL. 9, NO. 4, PP. 57-71.

https://doi.org/10.22034/IRSRM.2026.579139.1077

Calibrating DFN Models with a New Fracture Intensity Measure and Conventional Field Surveys

Nima Babanouri[1]* ;Saeed Shiri-Samar[1]
1. Department of Mining Engineering, Hamedan University of Technology, Hamedan, Iran.

Received: 20 January 2026 Accepted: 20 March 2026
(*Corresponding author: babanouri@hut.ac.ir)

Keywords

Discrete Fracture Network (DFN),
Fracture Intensity,
Model Calibration,
Response Surface Methodology, Field Survey

Abstract

Discrete Fracture Network (DFN) models are critical tools in rock engineering for simulating the geometric characteristics of fracture systems. However, accurate DFN modeling is hindered by limitations in conventional survey methods, particularly linear scanlines, which often underrepresent fracture intensity. This study introduces a new metric, the Joint Presence Factor (P), to quantify fracture intensity through planar sampling. The metric represents the percentage of sampling apertures intersected by fractures on a survey plane, providing a dimensionless measure of fracture occurrence that is practical, spatially representative, and physically intuitive, while also being simpler to measure and interpret than established fracture intensity indices. Alongside the field calculation of P in a case study, this metric was also calculated within DFN models through a custom FISH code. Using response surface methodology, the key DFN parameters, including fracture length, scaling exponent, and frequency, were optimized within the proposed calibration framework to align the model-derived P with field observations. The results demonstrated that the initial DFN model underestimated fracture intensity (P =14%) compared to field measurements (P =21%), reflecting the limitations of scanline surveys. After calibration, the optimized model yielded P =20%, showing good agreement with field data. The results indicated that adjusting fracture length distribution and intensity improves the representation of smaller fractures and enhanced overall network density, thereby increasing the reliability and accessibility of DFN models for rock engineering applications

1- Introduction

Rock discontinuities are among the key features in rock engineering studies. These discontinuities directly affect the mechanical behavior of the rock mass. These effects include changes in the strength, permeability, and deformability of the rock mass. Therefore, precise surveying and modeling of these discontinuities are essential for any mining and construction project involving rock.

Discrete Fracture Network (DFN) models explicitly represent the geometry of individual rock fractures as discrete planar features in three dimensions. These models are inherently stochastic in practice, with fracture attributes such as orientation, length, and intensity sampled from statistical distributions derived from field data [1, 2]. This approach allows DFNs to realistically simulate the complex heterogeneity of natural fracture systems, making them invaluable in geomechanical and hydrogeological modeling [3–6].

However, the accuracy of DFN models largely depends on the quality of the input data. Calibration is critical to DFN modeling as it ensures that the simulated fracture networks match real-world conditions. High-resolution techniques such as terrestrial laser scanning, borehole televiewers, and aerial photogrammetry offer detailed spatial information, significantly improving fracture identification and parameterization [7–10]. In addition, microseismic monitoring during hydraulic stimulation provides insight into active fracture geometry, helping constrain DFN structure in three dimensions [11, 12].

Many of the advanced methods for gathering high-resolution data are expensive and require specialized equipment that may not be accessible in many practical situations. In such cases, more conventional methods such as scanline and planar surveys have gained attention as they allow to acquire a continuous and statistically representative measurement of fractures along predetermined lines or surfaces on rock exposures [13]. However, these conventional

techniques come with their own set of limitations, particularly in accurately capturing fracture lengths and frequency. This makes calibration even more important, as errors in the initial data can propagate through the model, affecting its overall reliability [14, 15].

This study aims to improve the calibration of DFN models using data from conventional field techniques, demonstrated through a case study. A new metric, the Joint Presence Factor (*P*), is introduced to quantify fracture intensity based on the proportion of intersected sampling windows on a survey plate. In the field surveys, the survey plate consisted of a transparent physical sampling plate placed directly on the rock surface. An equivalent virtual survey plane was later implemented within the DFN model to calculate the Joint Presence Factor numerically. The DFN model was calibrated by adjusting key parameters through Response Surface Methodology (RSM) to match the field-derived joint presence factor. This methodology improves the realism and reliability of DFN models and offers a practical solution for rock engineering projects.

2- Linear survey of rock mass discontinuities

The study area is located at the Baba-Ali iron ore mine, situated in western Iran (Fig. 1a). The geology of the mine area is primarily composed of sedimentary formations, including sandstones and iron-rich units, with magnetite being the main ore mineral. Developing a calibrated three-dimensional model of the rock mass discontinuities is crucial for optimizing design and anticipating operational challenges within the mine. This study focuses specifically on the waste rock mass, which constitutes a substantial portion of the benches and final pit walls due to its non-extractive nature and also serves as a structural base for mine development. The investigated rock mass is exposed along a bench outcrop with an average slope of 80° on the western wall of the open pit (Fig. 1b).

The scanline survey method was used to systematically record discontinuities across the rock mass outcrop at the Baba-Ali mine. This method involves identifying, measuring, and documenting all visible fractures that intersect a linear reference line laid out on the rock surface [16]. It provides a statistically significant dataset that forms the basis for the development of an initial DFN model.

To construct a reliable DFN model, it is essential to establish accurate initial parameters, including spatial orientation, discontinuity length distribution, and fracture intensity. A total of 92 meters of linear surveys were conducted across 20 scanlines along the western wall of the mine (Fig. 1a). Each scanline was placed horizontally with lengths ranging from 1 to 6 meters to accommodate outcrop constraints, visibility, and safe access conditions. A clinorule was used in combination with a total station survey system, which allowed for precise angular measurements of discontinuity orientations in an environment where magnetic compasses are unreliable due to local magnetic anomalies typical of iron ore deposits, to measure discontinuity orientation.

Fig. 1. Linear survey of discontinuities: a) location of Baba-Ali iron ore mine in western Iran, b) overview of open-pit mine showing scanline survey area along western wall, c) scanline placement and clinorule used for measuring orientation and dip of rock joints

The data collected are visualized in the stereographic projection presented in Fig. 2. Joint sets 1, 2, and 3, together with the background fractures, were represented by 37, 54, 36, and 38 measured fractures, respectively. Sampling biases may exist if the scanline's orientation is not optimal with respect to the dominant fracture sets, and these biases must be corrected using stereological methods. To adjust for orientation bias in data collection, Terzaghi weighting was applied in the stereographic analysis [17]. This correction method compensates for the likelihood that certain joints intersect the scanline at higher frequencies due to their orientations. This correction ensures that joints intersecting the scanline at lower angles, which have a reduced chance of being sampled, are not under-represented in the dataset, thus improving the reliability of the stereographic analysis. Three joint sets were identified using the cluster analysis feature in Dips v.7, which applies fuzzy

clustering algorithms to group orientation data. The sets identified through this method are shown in Fig. 2, along with background or non-systematic joints.

The Fisher distribution was employed to characterize the spatial dispersion of fracture orientations around the mean dip and dip direction of each joint set. In this distribution, the concentration parameter K quantifies the degree of clustering: higher K values indicate a tighter concentration of fractures around the mean orientation. The K values were determined for each joint set based on the clustering analysis of field measurements. Table 1 presents the mean dip, dip direction, and corresponding K values for the identified joint sets.

Background joints, which do not cluster into distinct sets, were introduced into the model using a bootstrapping method. This method involves generating each background joint by randomly replacing one of the rows of recorded data for these joints, effectively recreating the background fractures without clustering.

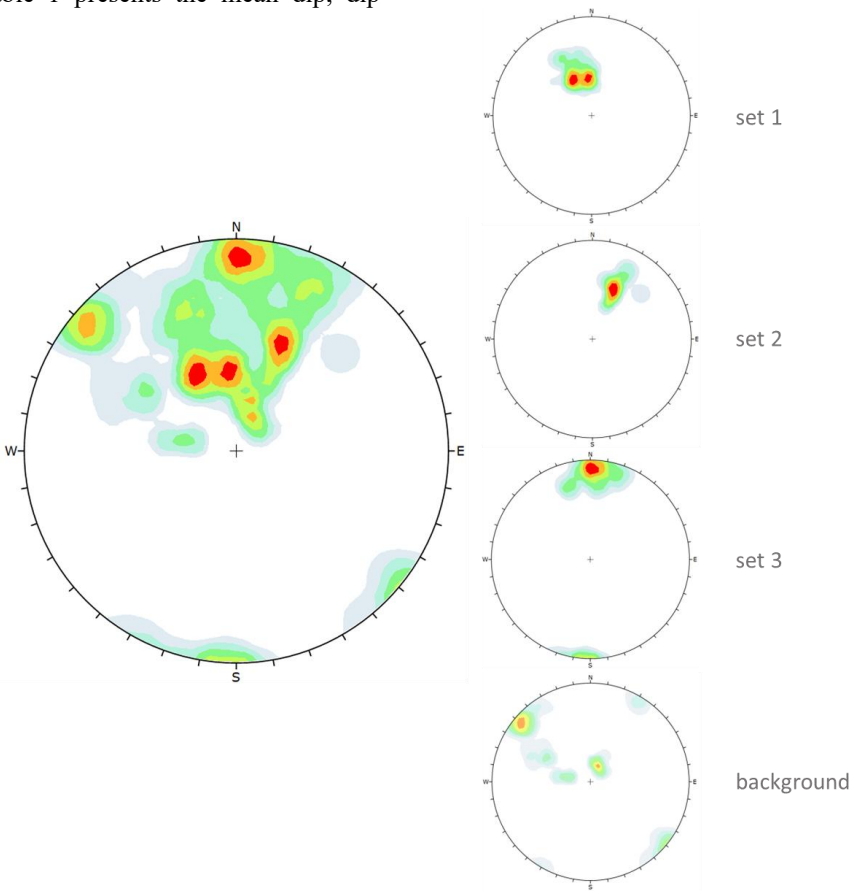

Fig. 2. Stereographic projection of joint orientation data corrected using Terzaghi weighting. Left panel shows density contour plot of all recorded discontinuities, highlighting dominant joint orientations. The right panels display individual joint sets (sets 1–3) identified through cluster analysis, along with background joints that do not belong to any dominant set.

Measuring trace length in the linear survey posed challenges, especially where discontinuities were only partially visible due to outcrop limitations. For fractures where only one end was visible, the trace length (L) was approximated by averaging the lengths of similar fractures within the same joint set. In cases where fractures extended beyond the observable area at both ends, the visible portion was taken as the full length. This inherent uncertainty in trace length determination introduces a source of error in the DFN model, highlighting the importance of subsequent model calibration and validation to mitigate inaccuracies resulting from incomplete observations.

To express variations in fracture length, a power-law distribution was used due to its widespread application in DFN modeling and its ability to capture the natural heterogeneity of fracture systems. Although the observed fracture lengths covered a relatively limited range, power-law distributions can still represent

truncated fracture size distributions commonly observed in natural rock masses. In particular, the Power-law distributions effectively describes the heavy-tailed nature of fracture lengths (Eq. 1).

$$n(L) = \lambda \ L^{-a} \quad (1)$$

where $n(L)$ is the number of fractures of length L, λ represents the normalization constant tied to total fracture abundance, and a is the scaling exponent that defines the size distribution of fractures. The scaling exponent was estimated for joint sets 1, 2, and 3, as well as the background fractures, with coefficients of determination (R^2) of 0.89, 0.84, 0.83, and 0.86, respectively. The scaling exponent and fracture length bounds used for joints in the study area are summarized in Table 1.

Fracture intensity for each joint set and the background joints was quantified using the linear intensity metric $P10$, which represents the number of fractures intersecting a unit length of scanline (measured in m^{-1}). The $P10$ values in Table 1 reflect the average fracture density across the total scanline lengths for each identified set. These values are critical in generating the DFN model, as they control the spatial frequency of fractures along the scanline and influence the probability of fracture occurrence during stochastic model generation.

3- Introduction of new measure of fracture intensity

Fracture intensity quantifies how extensively fractures intersect a rock mass, which is critical for assessing fluid flow, strength, and deformation characteristics. In traditional scanline surveys, fracture intensity is represented by the $P10$ parameter. However, due to the linear nature of the method, short fractures or those intersecting the scanline at small angles have a reduced probability of being recorded. As a result, using scanline data alone for constructing a DFN model may not capture the full complexity of the fracture system. To address limitations of scanline survey, a complementary planar survey was conducted to calibrate and enhance the initial DFN model derived from scanline data.

In this study, an efficient method for measuring and expressing areal fracture intensity was developed. For this purpose, a custom-designed survey plate was used to enable practical data collection. The survey plate consisted of a transparent plastic sheet measuring 1 meter by 1 meter, featuring circles with diameters of 1 and 3 centimeters arranged on a grid of points spaced at 10-centimeter intervals. The plate was placed directly on the rock outcrop, and the number of circles intersected by fractures was counted (Fig. 3). Separate counts were taken for the 1 cm and 3 cm circles.

The joint presence factor (P) is introduced as the ratio of the number of circles intersected by at least one fracture to the total number of circles on the survey plate, expressed as a percentage. This metric serves as a dimensionless measure for fracture intensity, based on the assumption that the more fractured the rock surface, the higher the probability that any given circular aperture will intersect a fracture. the joint presence factor simplifies data acquisition, provides a spatially distributed estimate of fracture occurrence, and minimizes subjectivity while increasing reproducibility. Moreover, its percentage-based definition gives it a tangible and intuitive interpretation, making it well suited for both practical field use and model calibration.

A total of 18 planar surveys were conducted, yielding average joint presence factors of 18.78% for 1 cm apertures and 20.67% for 3 cm apertures (Table 2). While standard deviations were observed across both datasets, the coefficients of variation, which express relative variability, were 68% for P_{1cm} and 33% for $P_{(3cm)}$. The higher variability in $P_{(1cm)}$ indicates greater sensitivity to local heterogeneity at smaller scales. Accordingly, $P_{(3cm)}$ was selected as the primary fracture intensity index and is referred to as P hereafter. This index served as a key input for calibrating the DFN model to better align with field-observed fracture densities.

Table 1. Initial DFN parameters for joints in the rock mass.

Fracture group	set 1	set 2	set 3	background
Dip (°)	47.8	58.0	80.4	
Dip direction (°)	161.7	205.6	181.9	bootstrapped
Fisher's K parameter	28.8	35.1	34.6	
L_{min} (m)	2.4	2.2	2.1	2.1
L_{max} (m)	19.7	12.6	13.6	22.9
Fracture size scaling exponent a	1.03	1.21	1.01	1.03
Fracture intensity $P10$ (m^{-1})	0.40	0.59	0.39	0.41

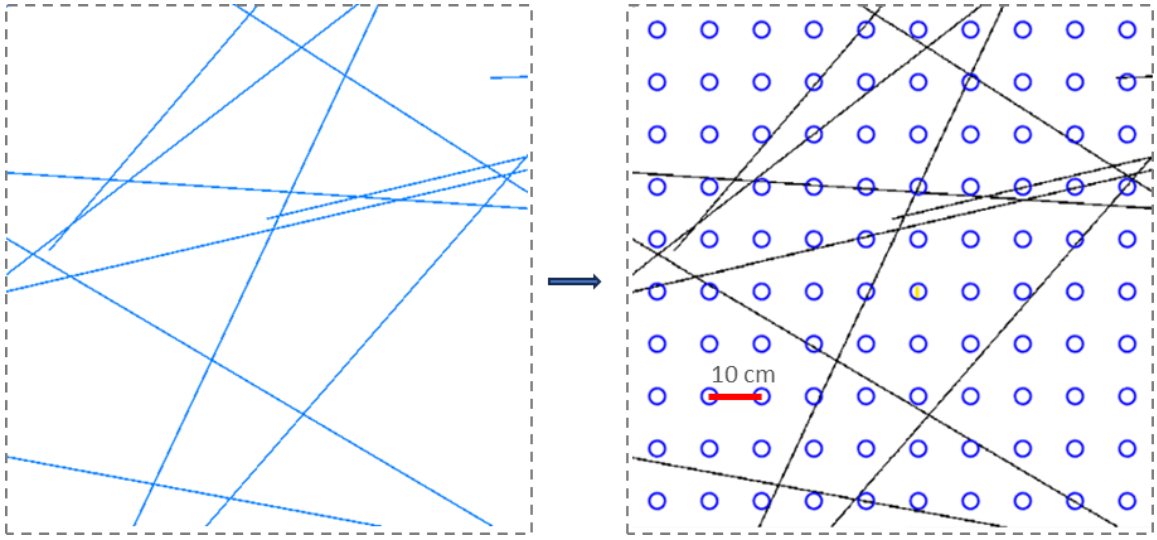

a)

b)

c)

Fig. 3. Method for measuring fracture intensity using joint presence factor (*P*): a) Schematic illustration showing transition from a fracture trace map (left) to a grid of circular sampling windows (right) used to compute *P*, b) Field example of circular apertures (1 cm and 3 cm diameters), c) Transparent survey plate placed over rock outcrop

.

4- DFN calibration

4-1- Initial DFN model construction

The three-dimensional DFN model was developed using 3DEC v.7, focusing solely on the geometric characterization of the rock mass rather than its mechanical or hydraulic behavior. Based on linear survey data and the DFN parameters listed in *Table 1*, an initial discrete fracture network was generated for the study area within a 50 m × 50 m × 50 m domain (Fig. 4). The initial DFN established in this step served as the baseline model for further calibration. However, to enhance the model's accuracy, it was necessary to refine it using additional field-derived data.

4-2- Calculating joint presence factor in DFN model

To quantify fracture intensity in the DFN model, the joint presence factor was calculated using a custom FISH function. This factor represents the percentage of sampling circles on a virtual survey plate that are intersected by at least one fracture trace. The method replicates the physical survey approach using circular

Table 2. Joint presence factor obtained from planar surveys using 1 cm and 3 cm apertures, with summary statistics across 18 locations.

Sample No.	$P_{(1cm)}$ (%)	$P_{(3cm)}$ (%)
1	57	18
2	39	14
3	10	16
4	13	21
5	12	16
6	15	19
7	26	31
8	38	42
9	17	22
10	11	21
11	12	15
12	13	19
13	7	10
14	13	23
15	21	26
16	10	21
17	13	21
18	11	17
Average	18.78	20.67
Standard Deviation	12.81	6.90
Coefficient of Variation (%)	68	33

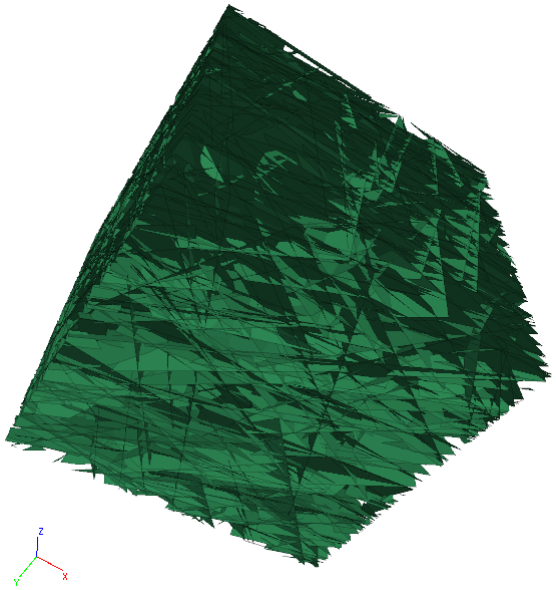

Fig. 4. Initial three-dimensional DFN model of the studied rock mass within a 50 m cubic domain.

sampling windows, but within a numerical model for consistency and calibration. The main steps are:

I. Defining the survey plate orientation and size
The plate is defined by its center coordinates, dip, and dip direction, which are converted into a plate normal vector. This vector orients the plate in 3D space. The plane width, grid spacing, and circle diameter are also specified.

II. Creating the survey plate geometry
Using the specified center and orientation, four corner points are calculated to construct a square plate. A polygon is formed in 3DEC using these points to define the survey surface.

III. Identifying fractures that intersect the plate
The function loops through all DFN fractures and checks for intersection with the survey plate polygon. Only those fractures that intersect the plate are stored for further checks. This step optimizes performance by reducing unnecessary intersection tests.

IV. Setting up grid points and circular sampling areas
A grid is laid over the plate, with points spaced according to the defined grid spacing. At each grid point, a circular sampling window (approximated by an octagon) is constructed using trigonometric geometry. The vertices of the polygon are projected onto the plate's plane to ensure they lie flat.

V. Checking for fracture intersections
Each sampling circle is tested for intersection with the list of pre-filtered fractures. If any fracture intersects the circle, the grid point is marked as intersected. Only the first detected intersection is recorded to avoid overcounting.

VI. Calculating the joint presence factor
After evaluating all grid points, the joint presence factor is calculated the percentage of intersected grid points out of the total grid points on the plate.

The FISH code is provided in the appendix. By calculating P, this approach allows for a systematic evaluation of fracture intensity on a virtual plane within the DFN model, aligning with field observations and enabling accurate DFN calibration.

A total of 20 virtual surveys were conducted within the DFN model, with each plane matching the orientation of corresponding field-based survey plates. These simulations produced an average model-derived joint presence factor of 13.86%. In contrast, the field-based surveys yielded a significantly higher average value of 20.67%.

The initial DFN model was generated using data from linear scanline surveys, which may underrepresent fracture intensity due to the inherent sampling limitations of scanlines and uncertainties associated with censored fracture lengths. As a result, the model underestimates the overall fracture intensity. This

discrepancy indicates that the DFN model, as currently configured, does not fully replicate the fracture intensity observed in the field, underscoring the need for calibration.

4-3- Calibration of DFN parameters

In this study, fracture length and frequency were selected as the key parameters for DFN model calibration. The fracture length distribution was characterized by three parameters: minimum length (L_{min}), maximum length (L_{max}), and the scaling exponent (a) of the power-law distribution. Fracture frequency was defined using the linear intensity parameter $P10$. These four parameters were adjusted during calibration to better align the model output with observed field data.

Fracture length and frequency were prioritized for calibration because they are particularly susceptible to underestimation in linear scanline surveys. Shorter fractures, in particular, have a lower probability of intersecting the scanline and may go unrecorded, especially if they are oriented at low angles relative to the scanline direction. As a result, the initial $P10$ values derived from the scanline survey may not accurately reflect the true fracture intensity of the rock mass. Additionally, due to the limitations of the linear method in fully capturing the variability in fracture length, the associated power-law parameters may also require adjustment to match the spatial fracture patterns observed in more comprehensive field or virtual surveys.The main idea of the calibration process was to adjust the values of these variables so that the joint presence factor in the DFN model matches the actual value. Instead of using a trial-and-error approach, a systematic approach was used to analyze the impact of changes in each calibration parameter on the model response.

To systematically explore the effects of calibration variables, a Design of Experiments (DOE) approach was employed, specifically using Response Surface Methodology (RSM) [18]. RSM enables efficient exploration of the parameter space by constructing a mathematical surface that approximates the model response, the joint presence factor in here, as a function of selected calibration variables. This approach optimizes computational resources while enabling a detailed analysis of how variations in joint length and frequency affect the DFN model.

In this study, response surface analysis was conducted using Design-Expert software, and all calibration parameters were adjusted through dimensionless scale factors. The minimum and maximum fracture lengths (L_{min} and L_{max}) were scaled using a common length factor (L^*), which was varied from 0.25 to 2. This allowed for both reduction and amplification of the original values derived from scanline surveys, enabling a broader representation of fracture sizes across the DFN model.

The fracture length distribution exponent a was similarly calibrated using a dimensionless scaling factor (a^*) ranging from 1 to 5. Given that the initial a values obtained from linear sampling were close to 1, multiplying by a^* produced final values spanning from 1 to 5, aligning well with the commonly reported range for natural fracture networks [19, 20]. This range encompasses both heavy-tailed and truncated length distributions and supports more realistic modeling of heterogeneous fracture systems.

Finally, $P10$ was calibrated using the scale factor $P10^*$, which was varied between 0.25 and 3. This range allowed the model to explore a wide spectrum of fracture densities while maintaining the relative relationships among the different joint sets. Together, these dimensionless scaling factors ensured a flexible yet coherent calibration framework for improving DFN model fidelity.

A total of 17 experiments were generated through the DoE framework to investigate the effect of these variables. For each experiment, a DFN model was generated with the adjusted parameters, and the average value of P was computed for evaluation (Table 3).

Subsequently, a nonlinear statistical model was fitted to describe the response surface of P as a function of the calibration variables. The p-value was used to assess the statistical significance of each term in the regression model; lower p-values indicate higher statistical significance. High coefficients of determination values confirmed the strong predictive capability of the fitted model, demonstrating its effectiveness in capturing the relationship between calibration parameters and the DFN model response (Table 4).

Once the response surface model was constructed, it was used to identify the combination of input variables that most closely matched the target response. This is done by analyzing the gradients and curvatures of the fitted surface to locate the optimum point [18, 21]. The goal was to identify the optimal combination of calibration variables that would yield a model-derived P close to the target field value of 20.67%, as measured during the planar surveys.

The optimization output suggested a combination of L^*=1.14, a^*=2.78, and $P10^*$=1.20. When these parameters were applied to the DFN model, the resulting average joint presence factor was P=20%, which is in close agreement with the field measurement. This minor discrepancy likely results from idealizations in the modeling approach, such as the assumption of uniform fracture properties across the rock mass. Nevertheless, the calibrated model

Table 3. DOE and DFN model response in terms of joint presence factor

Run	Model design			Model response
	a	L^*	$P10^*$	P (%)
1	3	2.0	0.25	4.22
2	5	1.25	0.25	5.13
3	3	1.25	1.625	26.33
4	5	1.25	3.0	30.63
5	3	0.25	0.25	3.36
6	5	0.25	1.625	22.78
7	1	1.25	3.0	36.98
8	3	2.0	3.0	39.57
9	3	0.25	3.0	34.36
10	3	1.25	1.625	26.17
11	3	1.25	1.625	26.30
12	1	0.25	1.625	20.55
13	1	2.0	1.625	26.89
14	5	2.0	1.625	25.63
15	3	1.25	1.625	26.14
16	3	1.25	1.625	26.69
17	1	1.25	0.25	3.56
Min.	1	0.25	0.25	3.36
Max.	5	2.0	3.0	39.57

provides a reliable representation of fracture intensity for practical engineering and geomechanical analysis.

A comparative evaluation of the initial and calibrated DFN parameters reveals how the optimization process altered the fracture network structure (Table 5). The scaling exponent a underwent the most pronounced change, increasing from values near 1.0–1.2 to 2.8–3.35 across all joint sets. This adjustment addresses the inherent underestimation of small fractures in linear scanline surveys, where shorter fractures are less likely to be recorded. The calibrated values better reflect the true fracture size distribution, enhancing the model's capacity to represent natural heterogeneity.

The $P10$ values also increased across all sets, most notably in set 2, where it rose from 0.59 to 0.71 m^{-1}. This signifies a denser fracture network, which directly contributes to a higher joint presence factor by increasing the number of intersections with sampling windows.

Adjustments in fracture length bounds further improved the model's accuracy. L_{min} increased modestly (e.g., 2.2 m to 2.5 m in set 2), while L_{max} showed moderate gains (e.g., 19.7 m to 22.5 m in set 1). The upward shift in L likely compensates for the recalibrated power-law distribution while preserving geologically realistic fracture dimensions.

Table 4. Regression coefficients and fit statistics for the response surface model of joint presence factor as a function of calibration variables.

Term	Coefficient	p-value
Intercept	26.41	—
a	-1.20	0.0090
L^*	1.19	0.0093
$P10^*$	15.66	<0.0001
$a \times P10^*$	-1.98	0.0037
$L^* \times P10^*$	1.09	0.0619
a^2	-1.11	0.0527
$(P10^*)^2$	-6.13	<0.0001
Model Fit Statistics		
R^2		0.9957
Adjusted R^2		0.9924
Predicted R^2		0.9634

Collectively, these adjustments improved the DFN model's ability to simulate the observed fracture

intensity by increasing both the number and the effective size distribution of fractures intersecting the survey areas. The result is a more connected and geologically representative fracture network.

A visual comparison between the initial and calibrated DFN models is shown in Fig. 5, which presents two cross-sections (each 10 meters long) from the same position in the rock mass. The calibrated model exhibits a denser and more spatially distributed fracture pattern compared to the initial configuration, in agreement with the quantitative improvements in P values.

5- Conclusions

This study introduced a systematic calibration framework based on the joint presence factor, a probability-based metric developed to express fracture intensity in a reproducible and spatially representative manner. The joint presence factor is defined as the percentage of circular apertures on a survey plate that intersect at least one fracture trace. This simplifies field data acquisition while retaining meaningful representation of fracture distribution.

The joint presence factor offers several key advantages that enhance both practical and analytical aspects of DFN modeling. By expressing fracture intensity as a percentage, the metric has a tangible and intuitive interpretation that aligns well with common engineering reasoning. Because the joint presence factor is derived from planar sampling rather than a single linear scanline, it is less sensitive to orientation-related sampling bias and provides a more spatially representative estimate of fracture occurrence. Unlike line-based measures such as $P10$, the proposed metric is plane-based and therefore better captures the spatial distribution of fractures. In addition, compared with more complex measures such as $P21$ and $P32$, it is simpler to measure and interpret while remaining dimensionless and physically intuitive.

Its use is not restricted to low-resolution or conventional data; rather, it provides a flexible tool that can be equally integrated with high-resolution digital outcrop models, borehole images, or LiDAR-derived fracture maps. This approach minimizes subjectivity by reducing reliance on manually measured parameters and operator interpretations.

In this study, the uncertainty associated with the initial scanline-derived DFN parameters, including the effects of censored fractures and the sampling bias inherent in linear scanline surveys, was managed through systematic calibration against the field-derived Joint Presence Factor. Model validation was performed by evaluating the ability of the calibrated DFN to reproduce the fracture intensity observed in the outcrop surveys.

The DFN model prior to calibration was constructed using data from linear scanline surveys. As a consequence, the resulting model significantly underestimated fracture intensity, as evidenced by a model-derived joint presence factor (P = 14%) that fell well below the field-based measurement (P = 21%). This discrepancy highlighted a key limitation in transferring raw field measurements into reliable DFN realizations without targeted calibration.

To address this gap, a response surface methodology was applied to systematically adjust DFN parameters and quantify their effect on P. Calibration was performed through dimensionless scaling of three core parameters: fracture length bounds (L_{min} and L_{max}, scaled by L^*), the power-law scaling exponent (a, scaled by a^*), and linear fracture intensity ($P10$, scaled by $P10^*$). This allowed the calibration process to preserve the relative differences among joint sets while optimizing the overall fit to field-derived intensity values. The optimization results produced a final model that closely approximated the observed fracture intensity, with P = 20%.

In conclusion, this study contributes a calibration methodology that promotes broader applicability of DFN modeling by making it more accessible to studies relying on conventional survey methods. The joint presence factor provides a practical link between field measurements and model parameters, enabling improved representation of fracture intensity within DFN models. Its integration into DFN workflows enhances the accessibility and consistency of DFN calibration. However, further applications in different geological settings would help assess its broader applicability.

Table 5. Comparison of initial and calibrated DFN parameters for each joint set in the rock mass (Arrows denote the change in value after calibration)

Fracture group	set 1	set 2	set 3	background
L_{min} (m)	2.4→2.7	2.2→2.5	2.1→2.4	2.1→2.4
L_{max} (m)	19.7→22.5	12.6→14.4	13.6→15.5	22.9→26.1
a	1.033→2.872	1.206→3.353	1.010→2.808	1.033→2.872
$P10$ (m^{-1})	0.40→0.48	0.59→0.71	0.39→0.47	0.41→0.49

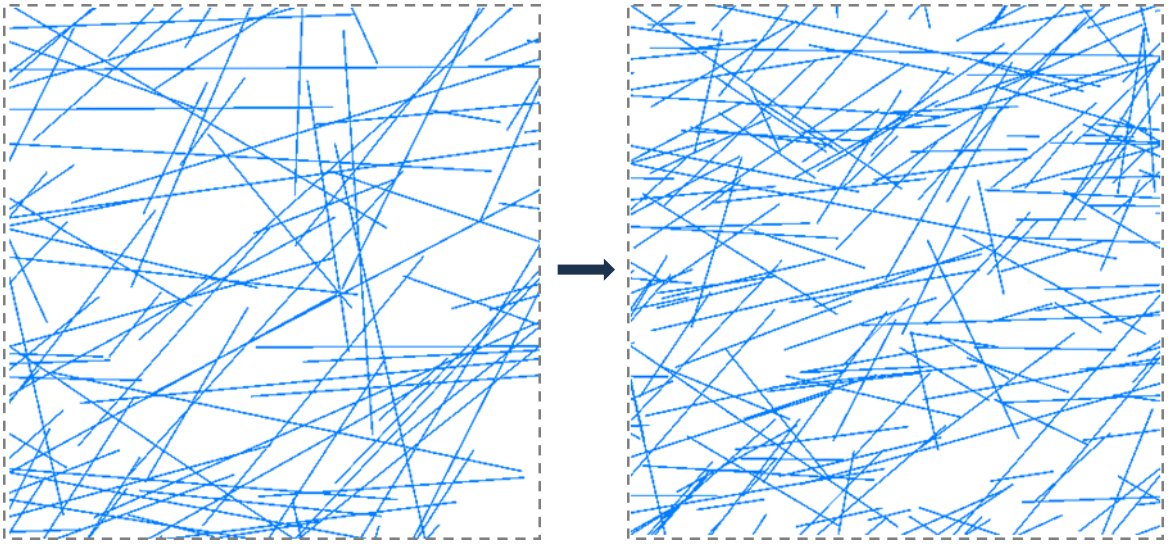

Fig. 5. Comparison between 2D sections of the initial DFN (a) and the calibrated DFN (b), each 10 meters in length.

References

[1] Dverstorp B, Andersson J (1989) Application of the discrete fracture network concept with field data: Possibilities of model calibration and validation. Water Resour Res 25:540–550. https://doi.org/10.1029/WR025I003P00540

[2] Cacas MC, Ledoux E, de Marsily G, et al (1990) Modeling fracture flow with a stochastic discrete fracture network: Calibration and validation: 2. The transport model. Water Resour Res 26:491–500. https://doi.org/10.1029/wr026i003p00491

[3] Lorig LJ, Darcel C, Damjanac B, et al (2015) Application of discrete fracture networks in mining and civil geomechanics. Min Technol 124:239–254

[4] Huang N, Liu R, Jiang Y, Cheng Y (2021) Development and application of three-dimensional discrete fracture network modeling approach for fluid flow in fractured rock masses. J Nat Gas Sci Eng 91:103957. https://doi.org/https://doi.org/10.1016/j.jngse.2021.103957

[5] Karimi-Fard M, Durlofsky LJ, Aziz K (2004) An efficient discrete-fracture model applicable for general-purpose reservoir simulators. SPE J 9:227–236

[6] Ren F, Ma G, Fan L, et al (2017) Equivalent discrete fracture networks for modelling fluid flow in highly fractured rock mass. Eng Geol 229:21–30

[7] Akara MEM, Reeves DM, Parashar R (2020) Enhancing fracture-network characterization and discrete-fracture-network simulation with high-resolution surveys using unmanned aerial vehicles. Hydrogeol J 28:

[8] Medinac F, Bamford T, Esmaieli K, Schoellig A (2018) Pre-and post-blast rock block size analysis using uav-lidar based data and discrete fracture network. In: ARMA International Discrete Fracture Network Engineering Conference. ARMA, p D023S008R002

[9] Mammoliti E, Pepi A, Fronzi D, et al (2023) 3D discrete fracture network modelling from UAV imagery coupled with tracer tests to assess fracture conductivity in an unstable rock slope: implications for Rockfall phenomena. Remote Sens 15:1222

[10] Cacciari PP, Futai MM (2017) Modeling a Shallow Rock Tunnel Using Terrestrial Laser Scanning and Discrete Fracture Networks. Rock Mech Rock Eng 50:1217–1242. https://doi.org/10.1007/s00603-017-1166-6

[11] Williams-Stroud SC, Eisner L (2010) Stimulated fractured reservoir DFN models calibrated with microseismic source mechanisms. In: ARMA US Rock Mechanics/Geomechanics Symposium. ARMA, p ARMA-10

[12] Zhou Z, Su Y, Wang W, Yan Y (2016) Integration of microseismic and well production data for fracture network calibration with an L-system and rate transient analysis. J Unconv Oil

Gas Resour 15:113–121. https://doi.org/https://doi.org/10.1016/j.juogr.2016.07.001

[13] Lepillier B, Bruna P-O, Bruhn D, et al (2020) From outcrop scanlines to discrete fracture networks, an integrative workflow. J Struct Geol 133:103992. https://doi.org/https://doi.org/10.1016/j.jsg.2020.103992

[14] Sewnun D, Wesseloo J, Heinsen Egan M (2022) A review of structural data collection methodologies for discrete fracture network generation. In: Caving 2022: Proceedings of the Fifth International Conference on Block and Sublevel Caving, Australian Centre for Geomechanics, Perth. pp 1047–1060

[15] Becker I, Koehrer B, Waldvogel M, et al (2018) Comparing fracture statistics from outcrop and reservoir data using conventional manual and t-LiDAR derived scanlines in Ca2 carbonates from the Southern Permian Basin, Germany. Mar Pet Geol 95:228–245

[16] ISRM (1978) Suggested Methods for the Quantitative Description of Discontinuities in Rock Masses. Rock Characterisation Test. Monit.

[17] Terzaghi RD (1965) Sources of error in joint surveys. Geotechnique 15:287–304

[18] Myers RH, Montgomery DC, Anderson-Cook CM (2016) Response surface methodology: process and product optimization using designed experiments. John Wiley & Sons

[19] Berkowitz B (2002) Characterizing flow and transport in fractured geological media: A review. Adv Water Resour 25:861–884. https://doi.org/http://dx.doi.org/10.1016/S0309-1708(02)00042-8

[20] Bonnet E, Bour O, Odling NE, et al (2001) Scaling of fracture systems in geological media. Rev Geophys 39:347–383

[21] Montgomery DC (2017) Design and analysis of experiments. Wiley

Appendix: Calculation of joint presence factor using FISH code

```
fish define calculate_joint_presence_factor

    ; Step I: Define survey plate orientation and size
    ; Inputs: plate center, dip, dip direction, plate width, grid spacing, and circle diameter
    ; Also calculates the plate normal vector for 3D orientation

    xc = 20
    yc = 20
    zc = 11
    dip = 80   ; Dip in degrees
    dip_dir = 90  ; Dip direction in degrees
    W = 1.0                ; Width of the survey plate (1 meter)
    circle_diameter = 0.03 ; Diameter of each circular window on the plate
    grid_spacing = 0.1     ; Spacing between circle centers on the survey plate

    grid_count = 0
    intersect_count = 0
    circle_radius = circle_diameter / 2.0

    ; Step II: Create the survey plate geometry
    ; Calculates the 3D coordinates of the four corners based on orientation
    ; Builds a polygon (the survey plate) using these corner points in 3DEC

    survey_plate = geom.set.create("SurveyPlate1")

    normal_x = math.sin(dip * math.degrad) * math.cos(dip_dir * math.degrad)
    normal_y = math.sin(dip * math.degrad) * math.sin(dip_dir * math.degrad)
    normal_z = math.cos(dip * math.degrad)
    plate_normal = vector(normal_x, normal_y, normal_z)

    half_width = W / 2.0
    cos_dip_dir = math.cos(dip_dir * math.degrad)
    sin_dip_dir = math.sin(dip_dir * math.degrad)
    cos_dip = math.cos(dip * math.degrad)
    sin_dip = math.sin(dip * math.degrad)

    corner1 = vector(xc - half_width * cos_dip_dir, yc - half_width * sin_dip_dir, zc)
    corner2 = vector(xc + half_width * cos_dip_dir, yc + half_width * sin_dip_dir, zc)
    corner3 = vector(xc + half_width * cos_dip_dir - W * sin_dip * sin_dip_dir,...
                     yc + half_width * sin_dip_dir + W * sin_dip * cos_dip_dir,...
                     zc - W * cos_dip)
    corner4 = vector(xc - half_width * cos_dip_dir - W * sin_dip * sin_dip_dir,...
                     yc - half_width * sin_dip_dir + W * sin_dip *
```

```
cos_dip_dir,...
                        zc - W * cos_dip)

       plate_polygon = geom.poly.create(survey_plate)
       geom.poly.add.node(survey_plate, plate_polygon, corner1)
       geom.poly.add.node(survey_plate, plate_polygon, corner2)
       geom.poly.add.node(survey_plate, plate_polygon, corner3)
       geom.poly.add.node(survey_plate, plate_polygon, corner4)
       geom.poly.add.node(survey_plate, plate_polygon, corner1) ; Close the
loop

       ; Step III: Identify fractures that intersect the plate
       ; Loops through all fractures in the DFN and stores only those that
intersect the plate polygon

       intersecting_fractures = array(100)
       num_intersecting_fractures = 0

       loop foreach frac fracture.list
           if fracture.gintersect(frac, survey_plate) then
               num_intersecting_fractures += 1
               intersecting_fractures(num_intersecting_fractures) = frac
           endif
       endloop

       ; Step IV: Set up grid points and circular sampling areas
       ; Generates a grid of sampling circle centers across the plate
       ; Approximates each circle with an octagon and projects it onto the
survey plane

       loop local ix (-W / 2 + grid_spacing / 2, W / 2, grid_spacing)
           loop local iy (-W / 2 + grid_spacing / 2, W / 2, grid_spacing)

               grid_x = xc + ix * cos_dip_dir - iy * sin_dip_dir
               grid_y = yc + ix * sin_dip_dir + iy * cos_dip_dir
               grid_z = zc
               grid_center = vector(grid_x, grid_y, grid_z)

               grid_count += 1
               intersects = false

               grid_circle      =      geom.set.create("GridCircle_"      +
string(grid_count))
               circle_polygon = geom.poly.create(grid_circle)

               num_points = 8
               loop local j (1, num_points)
                   angle = 2 * math.pi * j / num_points
                   px  =  grid_x  +  circle_radius  *  math.cos(angle)  *
cos_dip_dir - circle_radius * math.sin(angle) * sin_dip_dir
                   py  =  grid_y  +  circle_radius  *  math.cos(angle)  *
sin_dip_dir + circle_radius * math.sin(angle) * cos_dip_dir
                   pz = grid_z - circle_radius * math.sin(dip) * sin_dip_dir
- circle_radius * math.cos(dip)

                   vertex   =   project_onto_plane(vector(px,   py,   pz),
grid_center, plate_normal)
```

```
                    geom.poly.add.node(grid_circle, circle_polygon, vertex)
                endloop

                geom.poly.add.node(grid_circle,             circle_polygon,
project_onto_plane(vector(grid_x   +   circle_radius,   grid_y,   grid_z),
grid_center, plate_normal))

                ; Step V: Check for fracture intersections
                ; For each sampling circle, checks intersection with pre-
filtered fractures
                ; First valid intersection marks the circle as intersected

                loop local k (1, num_intersecting_fractures)
                    frac = intersecting_fractures(k)
                    if fracture.gintersect(frac, grid_circle) then
                        intersects = true
                        exit loop
                    endif
                endloop

                if intersects then
                    intersect_count += 1
                endif

                geom.set.delete(grid_circle)
            endloop
        endloop

        ; Step VI: Calculate the joint presence factor
        ; Computes percentage of intersected sampling circles out of the
total

        P = (intersect_count / grid_count) * 100.0
        io.out("Joint Presence Factor (P): " + string(P) + "%")

    end
    [calculate_joint_presence_factor]
```

نشریه‌ی مکانیک سنگ
JOURNAL OF ROCK MECHANICS
دوره نهم، شماره۴، زمستان ۱۴۰۴، صفحه ۵۷ تا ۷۱
https://doi.org/10.22034/IRSRM.2026.579139.1077

کالیبراسیون مدل‌های شبکه شکستگی مجزا (DFN) با استفاده از یک شاخص جدید شدت درزه‌داری و برداشت‌های متداول میدانی

نیما بابانوری [1*] ؛ سعید شیری ثمر [1]
۱-گروه مهندسی معدن، دانشگاه صنعتی همدان، همدان، ایران.

دریافت : ۱۴۰۴/۱۰/۳۰؛ پذیرش: ۱۴۰۴/۱۲/۲۹
(*نویسنده مسئول: babanouri@hut.ac.ir)

چکیده

مدل‌های شبکه شکستگی مجزا (DFN) ابزارهای کلیدی در مهندسی سنگ برای شبیه‌سازی ساختار هندسی شکستگی‌ها هستند، اما دقت آن‌ها به شدت به کیفیت داده‌های ورودی وابسته است. روش‌های متداول برداشت میدانی مانند اسکن‌لاین، به‌دلیل ماهیت خطی خود، شدت واقعی شکستگی را کمتر از مقدار واقعی برآورد می‌کنند. در این پژوهش، شاخصی جدید به نام ضریب حضور درزه (P) به‌عنوان معیاری بدون بعد و مبتنی بر برداشت سطحی معرفی شده است که شدت شکستگی را به‌صورت درصدی از تقاطع شکستگی‌ها با پنجره‌های نمونه‌برداری دایره‌ای بیان می‌کند. این شاخص هم در برداشت‌های میدانی و هم در مدل DFN با استفاده از کدنویسی FISH محاسبه شده است. برای کالیبراسیون مدل، از روش سطح پاسخ (RSM) استفاده شد تا پارامترهای کلیدی شامل طول شکستگی، نمای توزیع و شدت خطی (P10) بهینه‌سازی شوند. نتایج نشان داد که مقدار P در مدل اولیه کمتر از مقدار میدانی است، اما پس از کالیبراسیون، تطابق قابل قبولی حاصل می‌شود. این روش، چارچوبی عملی و قابل اتکا برای بهبود دقت مدل‌های DFN فراهم می‌کند.

واژگان کلیدی

شبکه شکستگی مجزا (*DFN*)، شدت درزه‌داری، کالیبراسیون، روش سطح پاسخ (*RSM*)، برداشت میدانی درزه‌ها